ANGPTL4-Mediated Promotion of Glycolysis Facilitates the Colonization of *Fusobacterium nucleatum* in Colorectal Cancer

Xin Zheng[1,2], Rui Liu[1], Chenchen Zhou[1], Haopeng Yu[3,4], Wanyi Luo[1], Jianhui Zhu[1,2], Jiaxin Liu[1,2], Zhe Zhang[5], Na Xie[5], Xian Peng[1], Xin Xu[1,2], Lei Cheng[1,2], Quan Yuan[1], Canhua Huang[5], and Xuedong Zhou[1,2]

ABSTRACT

Colorectal cancer is a severe health problem worldwide, and accumulating evidence supports the contribution of *Fusobacterium nucleatum* (*F. nucleatum*) to colorectal cancer development, metastasis, and chemoresistance. However, the mechanisms underlying the colonization of *F. nucleatum* in colorectal cancer tissue are not yet clarified. Here we demonstrate that *F. nucleatum* infection mediated elevation of angiopoietin-like 4 (ANGPTL4) expression. Upregulated ANGPTL4 promoted glucose uptake and glycolysis activity in colorectal cancer cells *in vitro* and *in vivo*, which are necessary for the colonization of *F. nucleatum*. Furthermore, overall increased acetylation of histone H3 lysine 27 was observed in *F. nucleatum*–infected colorectal cancer cells and patient tumors, which was responsible for the corresponding transcriptional upregulation of ANGPTL4. These data indicate that the metabolic reprogramming of cancer cells induced by *F. nucleatum* is essential for its enrichment and persistence in colorectal cancer, providing a novel potential target for the clinical intervention of *F. nucleatum*–related colorectal cancer.

Significance: *F. nucleatum* colonization in colorectal cancer is regulated by ANGPTL4-mediated glycolysis, suggesting that this axis could be targeted for combined repression of *F. nucleatum* and cancer progression.

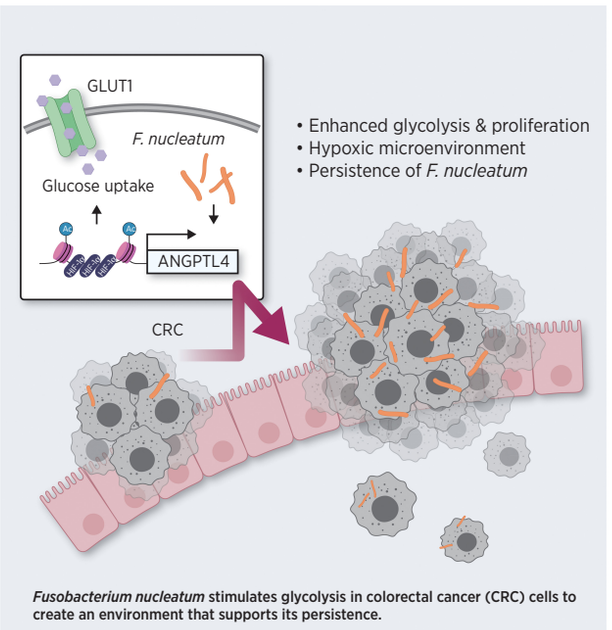

Fusobacterium nucleatum **stimulates glycolysis in colorectal cancer (CRC) cells to create an environment that supports its persistence.**

Introduction

Colorectal cancer is one of the most prevalent malignant tumors and the third leading cause of cancer mortality worldwide, characterized with poor prognosis and high metastasis (1). As a multifactorial disorder, colorectal cancer initiation and progression has been shown to be influenced by gut microbiota (2). In particular, many studies have consistently detected the enrichment of Fusobacterium spp. in colorectal cancer tissue compared with adjacent noncancerous tissue (3–7). *Fusobacterium nucleatum* (*F. nucleatum*) is a common oral gram-negative anaerobe known as one of the key pathogens of periodontal disease (8), and accumulating evidences suggest its contribution in the development (9–12), metastasis (13–16), and chemoresistance (17, 18) of colorectal cancer. It has been demonstrated that metronidazole treatment suppressing *F. nucleatum* load could reduce colorectal cancer cell proliferation and overall tumor growth as well in xenograft-bearing mice (19). These observations argue for further investigation of antimicrobial interventions as a potential treatment for patients with *Fusobacterium*-associated colorectal cancer.

A study using an orthotopic graft model showed that *F. nucleatum* localized to colorectal cancer in an Fap2-dependent manner via a hematogenous route (20). In experiments using the genetic $Apc^{Min/+}$ model, oral instilled *F. nucleatum* accelerated the onset of colonic tumors and enriched in tumor tissue relative to adjacent normal

[1]State Key Laboratory of Oral Diseases and National Clinical Research Center for Oral Diseases, West China Hospital of Stomatology, Sichuan University, Chengdu, P.R. China. [2]Department of Cariology and Endodontics, West China Hospital of Stomatology, Sichuan University, Chengdu, P.R. China. [3]West China Biomedical Big Data Center, West China Hospital/School of Medicine, Sichuan University, Chengdu, China [4]Med-X Center for Informatics, Sichuan University, Chengdu, P.R. China. [5]State Key Laboratory of Biotherapy and Cancer Center, West China Hospital, and West China School of Basic Medical Sciences & Forensic Medicine, Sichuan University, and Collaborative Innovation Center for Biotherapy, Chengdu, P.R. China.

X. Zheng and R. Liu contributed equally to this article.

Corresponding Authors: Xuedong Zhou, Department of Cariology and Endodontics, West China School of Stomatology, Sichuan University, Chengdu 610041, China. E-mail: zhouxd@scu.edu.cn; and Canhua Huang, hcanhua@scu.edu.cn

Cancer Res 2021;81:6157–70

doi: 10.1158/0008-5472.CAN-21-2273

tissue (10), indicating a predilection of *F. nucleatum* to tumor tissue. Nonetheless, binding and evasion may not fully explain *F. nucleatum*'s tropism to colorectal cancer. Whether could *F. nucleatum* modulate the behaviors of tumor cells to favor its own survival remains poorly understood. A recent study has revealed that *F. nucleatum* promotes glycolysis activity in colorectal cancer cells and considers this metabolism reprogramming as a decisive factor for the promoting effects of *F. nucleatum* on colorectal cancer proliferation and aggressiveness (9). In contrast, the similar facilitation of proliferation was not observed in nonneoplastic cell lines (11). Therefore, it is plausible that the rapid proliferation of colorectal cancer cells supported by active glycolysis creates a hypoxic microenvironment to guarantee the persistence and replication of anaerobic *F. nucleatum* resides in the tumor tissues.

Here, we explored whether the enhanced glycolysis in colorectal cancer cells induced by *F. nucleatum* contribute to its intratumor survival advantage, as well as pro-oncogenic effects on colorectal cancer. By *in vitro* coculture assays, *in vivo* xenograft model and clinical tissue analysis, we demonstrated that the enrichment of *F. nucleatum* in colorectal cancer cells was related to its promoting effect toward glycolysis activity of tumor cells. Via facilitating acetylation of histone H3 lysine 27 (H3K27ac), *F. nucleatum* infection induced ANGPTL4 expression and subsequently enhanced glucose uptake, thus promoting glycolysis activity of colorectal cancer cells and its own colonization in colorectal cancer cells.

Materials and Methods

Cell and bacterium culture

Human colorectal cancer cell lines DLD1 (RRID: CVCL_0248), SW480 (RRID: CVCL_0546), HCT-116 (RRID: CVCL_0291), and HT-29 (RRID: CVCL_0320) were obtained from ATCC, and a normal human colon mucosal epithelial cell line NCM460 (RRID: CVCL_0460) was obtained from INCELL. Cells were routinely cultured in DMEM (Thermo Fisher Scientific) supplemented with 10% FBS at 37°C in a humidified 5% CO_2 atmosphere. When indicated, 10 mmol/L 2-deoxy-D-glucose (2DG; APExBIO), 5 μg/mL recombinant human ANGPTL4 (rhANGPTL4; R&D Systems), 1 μmol/L A-485 (MedChemExpress), or 2 μmol/L BAY-876 (MedChemExpress) was added into the cell cultures. Reagents used are listed in Supplementary Table S1. All the cell lines were authenticated by short-tandem repeat analysis. *Mycoplasma* infection was tested with the Mycoplasma PCR Detection Kit (Beyotime). Cell lines cultivated less than 15 passages since their procurement were used in the following experiments.

Fusobacterium nucleatum (ATCC 25586) and *Porphyromonas gingivalis* (ATCC 33277) were purchased from ATCC and cultured in brain heart infusion broth (BHI; Difco) supplemented with 1 μg/mL hemin (Sigma) and 1 μg/mL menadione (Sigma) at 37°C under anaerobic condition (90% N_2, 5% CO_2, 5% H_2). Planktonic growth of *F. nucleatum* was monitored by measuring the optical density at 600 nm (OD_{600nm}).

For coculture of bacteria and cells, cells were grown to >90% confluency, and then inoculated with *F. nucleatum* or *P. gingivalis* at a multiplicity of infection (MOI) of 10:1 for most of the *in vitro* assays, or otherwise as indicated. Before inoculation, overnight bacterial cultures were back-diluted 1:1,000 and grown to mid–exponential phase (~0.5 OD_{600nm}), centrifuged (2 min, 4°C, 12,000 rpm) and resuspended with PBS. Prior to extracellular acidification rate (ECAR) measurement, protein/chromatin/RNA extraction, glucose uptake assay and *in situ* histone deacetylases (HDAC) activity evaluation, the cocultures were treated with gentamicin (300 μg/mL) and metronidazole (200 μg/mL) for 1 hour (11) to eliminate residual or extracellular adherent bacteria. For FISH, this step was omitted.

Xenograft model

Male, 4-week-old BALB/c nude mice (RRID: IMSR_JCL:JCL:mID-0001) of were housed under specific pathogen–free conditions. All animal experiments were performed in accordance with the NIH guidelines for the care and use of animals in research and approved by the Institutional Animal Care and Use Committee at West China Hospital of Stomatology, Sichuan University. A total of 2×10^6 DLD1 cells in 100 μL PBS were injected subcutaneously into the axilla of each mouse. Seven days after injection, mice were randomly divided into indicated groups, which was blinded to the investigators who collected the samples and performed analyses. As indicated in different experiments, adeno-associated virus (AAV; 2×10^{10} genome copies) was given by intratumoral injection once a week, *F. nucleatum* (1×10^7 CFU) was given by multipoint intratumoral injection twice a week, and 2DG (1 g/kg) was given by intraperitoneal injection twice a week. The length (L) and width (W) of the tumor were measured every 4 days using a caliper and converted into tumor volume with the formula $W \times L^2/2$. After treatment for 3 weeks, mice were sacrificed by CO_2 euthanasia, subcutaneous tumors were collected for follow-up analyses.

The Cancer Genome Atlas analysis

Transcriptome data were derived from The Cancer Genome Atlas (TCGA) colon adenocarcinoma (COAD) cohort with 469 solid tumor tissues and 41 normal tissues. The mRNA expression levels of all samples, presented as counts of exon model per million mapped reads (CPM), were normalized with a GDCRNATools package in R version 4.0.2. *Fusobacterium* genus abundance of corresponding sample, calculated on the basis of transcriptome data, was acquired from Poore and colleagues' study (21). Spearman correlations between the expression levels of indicated genes and *Fusobacterium* genus abundance were performed with GraphPad Prism version 8.4.2. Survival plots of patients with high and low ANGPTL4 expression level (quartile group cutoff) were analyzed on GEPIA (http://gepia.cancer-pku.cn/).

Clinical tissues

Paraffin-embedded colon adenocarcinoma tissues ($n = 27$) were collected in West China Hospital, Sichuan University. All procedures were approved by the Institution Review Board of West China Hospital of Stomatology, Sichuan University. Written informed consent was obtained from all participants. Patients with a known synchronous cancer diagnosis or other cancer diagnosis within 5 years of the operation, or a history of radiotherapy or chemotherapy, were excluded. No antibiotics were given preoperatively. Patient information is listed in Supplementary Table S2.

FISH

F. nucleatum and cells cocultured in eight-well μSlide (Ibidi) were washed three times with PBS and fixed with PBS/4% paraformaldehyde (PFA) for 15 minutes at room temperature. Clinical colorectal cancer tissue slides were washed three times with PBS. FISH were performed as described previously (22). Cells and bacteria were permeabilized with PBS/0.1% Triton X-100 for 1 hour at room temperature, and with lysozyme (30 mg/mL; J&K Scientific) for 30 minutes at 37°C, followed by PBS washing. Samples were then serially dehydrated in ethanol (50%, 80%, and 100%; 3 minutes each), exposed to 100 μL hybridization buffer (0.9 M NaCl, 20 mmol/L Tris-HCl, 0.01% SDS, 20% formamide) containing FUS714 probe (23)

conjugated with Alexa Fluor 555 (200 nmol/L; Supplementary Table S1) and incubated at 46°C for 90 minutes. After hybridization, samples were immersed in washing buffer (20 mmol/L Tris-HCl, 5 mmol/L EDTA, 0.01% SDS, 215 mmol/L NaCl) for 15 minutes at 48°C, and then rinsed with PBS. 6-Diamidino-2-phenylindole (DAPI; Solarbio) in deionized water was used to visualize the nuclei.

The imaging was performed using a FLUOVIEW FV3000 confocal laser scanning microscope (Olympus Corp.). Z-series image stacks were captured with constant acquisition parameters (gain, offset, and pinhole settings) for every separated assay. Each sample was scanned at randomly selected positions. Bacterial quantification was performed using COMSTAT2 program (24) by calculating the *F. nucleatum* biomass of each image. For clinical colorectal cancer tissues, *F. nucleatum* abundance was determined with ImageJ by calculating the ratio of *F. nucleatum*–positive area to DAPI-positive area in percentage.

ECAR quantification

ECAR of colorectal cancer cells were measured with a Glycolysis Assay Kit (Abcam) according to the manufacturer's instruction. Briefly, cells with or without *F. nucleatum* were cultured in clear-bottomed black 96-well plates. CO_2 was purged prior to the assay by transfer the cell cultures to a CO_2-free incubator for 3 hours. Dynamic fluorescent signal representing the level of extracellular acidification was measured with Flexstation III (Molecular Devices) in TR-F mode (delay time 30 microseconds, gate time 100 microseconds, Ex 380 nm, Em 615 nm). Slope of the fluorescent signal curve was calculated by linear regression and considered as the ECAR, and the result of each well was then normalized to cell number (ECAR/10,000 cell). The relative ECAR were further normalized with the average of the control group taken as 1.

F. nucleatum abundance quantification

gDNA was extracted from xenograft tumors with an QIAamp DNA Mini Kit (Qiagen). The gDNA purity and concentration were measured by a NanoDrop 2000 spectrophotometer. gDNA from each sample was subjected to qPCR (qPCR) to determine the amounts of *F. nucleatum* by detecting the 16S rDNA, with human prostaglandin transporter (PGT) as the reference gene (primers are listed in Supplementary Table S1; ref. 3). Each reaction mixture (10 μL) contained 1× TB Green Premix Ex Taq (Takara), 50 ng gDNA, and forward/reverse primers (500 nmol/L each). qPCR amplification and threshold cycle (CT) value measurement was performed using a LightCycler 480 system (Roche). The relative *F. nucleatum* abundance compared with the control group were calculated by $2^{-\Delta\Delta CT}$ method.

RNA sequencing and analysis

Total RNA from DLD1 cultured with or without *F. nucleatum* were extracted and purified using MiniBest Universal RNA Extraction Kit (Takara) according to the manufacturer's instruction. RNA quality was determined by 2100 Bioanalyser (Agilent) and quantified using the NanoDrop 2000 spectrophotometer (Thermo Fisher Scientific). The cDNA library was prepared following the procedures of TruSeq RNA Sample Preparation Kit (Illumina) using 1 μg total RNA and applied to paired-end sequencing using the Illumina NovaSeq 6000 sequencer (2 × 150bp read length). The raw paired-end reads were trimmed, and quality controlled by SeqPrep (RRID: SCR_013004) and Sickle with default parameters. Then clean reads were separately aligned to reference genome with orientation mode using HISAT2 software (RRID: SCR_015530). The mapped reads of each sample were assembled by StringTie (RRID: SCR_016323) in a reference-based approach. The expression level of each transcript was calculated according to the fragments per kilobase million (FPKM) method. Essentially, differential expression gene (DEG) analysis was performed using the DESeq2 (RRID: SCR_000154) with q value (adjusted P value) ≤0.05, and fold change >1.5. In addition, gene set enrichment analysis (GSEA) was performed according to the instruction (25).

Knockdown and overexpression of ANGPTL4

The coding region of ANGPTL4 (NM_139314.3) was amplified and cloned into pcDNA3.1/Zeo(+) vector (Thermo Fisher Scientific) for the construction of eukaryotic expression plasmid. The lentivirus-delivered or AAV-delivered small hairpin RNA for ANGPTL4 knockdown (shANGPTL4; ref. 26), as well as the nontarget control (shCtrl) were constructed by Hippo Biotechnology. Lentivirus-delivered shRNA for SERPINE1 (target sequence acquired from Sigma, TRCN0000331004) and HIF1A (target sequence acquired from Sigma, TRCN000003810) were constructed by Hippo Biotechnology. The oligonucleotides used are listed in Supplementary Table S1.

For transient transfection, cells at ∼50% confluency were transfected with empty vector or ANGPTL4 expression plasmid using Lipofectamine 2000 (Thermo Fisher Scientific) according to the instructions. For shRNA knockdown of ANGPTL4, SERPINE1, or HIF1A in cell lines, DLD1 or SW480 were infected with lentivirus-delivered shRNA, alone with 8 μg/mL polybrene (Sigma). Infected cells were selected with 1 μg/mL puromycin. For *in vivo* assays, AAV-delivered shANGPTL4 or shCtrl was intratumorally injected to mice as aforementioned. The efficiencies of gene overexpression and shRNA knockdown were confirmed with qPCR and Western blotting.

qPCR

For mRNA expression level quantification, total RNA was extracted as aforementioned with its purity and concentration measured by a NanoDrop 2000 spectrophotometer. The cDNA was generated from 1 μg RNA using RT reagent Kit with gDNA Eraser (Takara), followed by qPCR amplification and threshold cycle value measurement using a LightCycler 480 system. Each reaction mixture (10 μL) contained 1× TB Green Premix Ex Taq, 0.5 μL cDNA, and forward/reverse primers (500 nmol/L each, listed in Supplementary Table S1). The expression level of target gene was calculated by $2^{-\Delta CT}$ method with GAPDH selected as internal reference.

Protein extraction and Western blotting

Total protein was extracted using cell lysis buffer (Beyotime) supplemented with 1% protease inhibitor cocktail (Beyotime), whereas nuclear protein was extracted with NE-PER Nuclear and Cytoplasmic Extraction Reagents (Thermo Fisher Scientific) according to the instructions. Histone was extracted using NETN buffer (50 mmol/L Tris-Cl pH 8.0, 100 mmol/L NaCl, 1 mmol/L EDTA, 0.5% NP-40) and 0.2M HCl with a standard protocol. The concentration of the extracted protein was examined by Enhanced BCA Protein Assay Kit (Beyotime). Proteins were electrophoresed through 10% or 12% SDS-PAGE gels and then transferred to PVDF membranes (Bio-Rad). The membranes were blocked with 5% nonfat powdered milk (Sangon Biotech) for 1.5 hours at room temperature and subsequently incubated with indicated primary antibodies overnight at 4°C. After washed with Tris buffered saline containing 0.1% Tween-20 (TBST), membranes were incubated with HPR-conjugated secondary antibodies for 1 hour at room temperature, followed by TBST washing. The signals were detected using Immobilon ECL Ultra Western HRP Substrate (Merck Millipore) and visualized with ChemiDoc XRS+ Imaging System (Bio-Rad). All antibodies used are listed in Supplementary Table S1.

Glucose uptake assay

Cells with indicated treatment were incubated with a fluorescent deoxy-glucose analog 2-NBDG (200 μmol/L; APExBIO) in glucose-free DMEM for 1 hour at 37°C, followed by thoroughly washing with PBS. The fluorescence was measured using Flexstation III with Ex 485 nm and Em 535 nm. Glucose uptake ability was represented by the fluorescent read normalized to the cell number (RFU/10,000 cells).

Chromatin immunoprecipitation and qPCR

Chromatin from 1×10^7 cells was cross-linked with 1% PFA (10 minutes at room temperature), extracted and fragmented using an EZ-Zyme Enzymatic Chromatin Prep Kit (Merck Millipore). The prepared chromatin was then immunoprecipitated by indicated primary antibodies (with rabbit IgG antibody as the negative control) using a Magna ChIP HiSens Kit (Merck Millipore) according to the manufacturer's instruction. Immunoprecipitated protein-DNA cross-link was reversed, and the DNA was purified using a MicroElute DNA Clean-Up Kit (Omega). Chromatin immunoprecipitation (ChIP) and qPCR (ChIP-qPCR) was carried out in a 10 μL reaction volume containing 1 μL DNA, 500 nmol/L forward/reverse primers and 1× TB Green Premix Ex Taq (Takara). Enrichment of indicated DNA region by immunoprecipitation was normalized with nonprecipitated DNA input using $2^{-\Delta CT}$ method (% input). The peak regions of H3K27ac level and HIF1α binding level within ANGPTL4 locus were determined with ChIP sequencing (ChIP-seq) datasets in Cistrome Data Browser (accession ID of 62255 and 90168, respectively). The CT values derived from isotype IgG negative controls all exceeded 45, indicating a negligible level of nonspecific DNA immunoprecipitation. All antibodies and primers used are listed in Supplementary Table S1.

IHC

IHC staining of H3K27ac in clinical colorectal cancer tissues was performed with a standard method. Samples were permeabilized with PBS/0.1% Triton X-100 for 1 hour and blocked with 1% BSA for another 1 hour at room temperature, followed by incubation with the H3K27ac primary antibody (Supplementary Table S1) overnight at 4°C and subsequently with the HRP-conjugated second antibody (Supplementary Table S1) for 1 hour at room temperature. The signals were detected with a diphenylene diamine (DAB) system (Catalog No. abs957; Absin). The nuclei were stained with hematoxylin. The percentage of IHC positive cells with strong (S%), moderate (M%), or weak (W%) intensity respectively was analyzed by an IHC profiler plugin (27) in ImageJ (RRID: SCR_003070). The IHC score for H3K27ac was calculated with the formula $3 \times S + 2 \times M + 1 \times W$.

HDAC activity measurement

Cells cultured with or without bacteria were treated with antibiotics as mentioned before, followed by *in situ* HDAC activity measurement with a FLUOR DE LYS HDAC Fluorometric Cellular Activity Assay Kit (Enzo Life Sciences).

In addition, nuclear proteins were extracted from these cells and subjected to HDAC activity evaluation with the same method. The conditioned supernatants derived from cells with indicated treatment were added into assay buffer during the incubation of recombinant HDAC1/HDAC2 (Proteintech) with assay substrates to investigate their effects on the activities of HDAC1/HDAC2. 1 μmol/L trichostatin A (TSA) supplied within the kit was used as a positive control for HDAC activity inhibition.

Statistical analysis

Statistical analyses were performed with the GraphPad Prism software (RRID: SCR_002798). All data were expressed as mean ± SEM or median ± interquartile range. Two-group comparison was performed by Wilcoxon rank-sum test. Multiple group comparisons were performed with Welch ANOVA test followed by Dunnett T3 multiple comparisons test to identify differences between indicated groups. Spearmen correlations were performed with GraphPad Prism. Data were considered significantly different if the two-tailed P value <0.05. Sample sizes were given in the figure legends. All experiments were repeated independently for two or three times.

Resource availability

Further information and requests for resources and reagents should be directed to and will be fulfilled by the lead contact, Xuedong Zhou (zhouxd@scu.edu.cn). All unique/stable reagents generated in this study are available from the lead contact with a completed Materials Transfer Agreement. RNA sequencing (RNA-seq) data have been deposited in the public Gene Expression Omnibus database (RRID: SCR_005012) with the accession number GSE175593.

Results

Enrichment of *F. nucleatum* in colorectal cancer cells is related with enhanced glycolysis

Given the enrichment of *Fusobacterium* genus in colon tumors versus adjacent normal tissue (**Fig. 1A**), we further explored whether coculture with colorectal cancer cells could favor the growth of *F. nucleatum*. After overnight coculturing under aerobic condition, significantly more intensive *F. nucleatum* staining in colorectal cancer cell lines (DLD1, SW480, HCT-116 or HT-29) were detected by FISH, compare with that of a nonmalignant colon epithelial cell line NCM460 (**Fig. 1B** and **C**). Real-time observation of the coculture revealed that *F. nucleatum* invaded into DLD1 cells within 4 hours, and both DLD1 and *F. nucleatum* could maintain proliferation during the coculture under aerobic condition (Supplementary Fig. S1). One of the best characterized metabolic feature in cancer cells known as the "Warburg effect" is that they primarily utilize glucose through glycolysis rather than oxidative phosphorylation for energy supply even under aerobic condition (28). As it has been documented that *F. nucleatum* abundance is correlated with high glucose metabolism in patients with colorectal cancer (9), we then tried to figure out whether active glycolysis of colorectal cancer cells was biologically associated with the colonization and growth of *F. nucleatum*. By quantification of ECAR, the promoting effect of *F. nucleatum* infection toward glycolysis activity was observed in DLD1 and SW480, but not in NCM460 (**Fig. 1D**). Treatment of 2DG, an inhibitor of glycolysis, largely abolished the colonization of *F. nucleatum* cocultured with DLD1 or SW480 (**Fig. 1E** and **F**), whereas did not disturb the planktonic growth of solely cultured *F. nucleatum* (**Fig. 1G**). In xenograft model, 2DG treatment remarkably reduced tumor growth (**Fig. 1H** and **I**) and the *F. nucleatum* load in tumors as well (**Fig. 1J**).

F. nucleatum promotes glycolysis via inducing ANGPTL4 expression in colorectal cancer cells

To determine the proglycolysis effect of *F. nucleatum* and the related mechanisms, we performed RNA-seq to compare the gene expression profiles of DLD1 cultured with or without *F. nucleatum*. GSEA revealed that several gene sets including Hallmark_Hypoxia and Hallmark_Glycolysis were enriched in DLD1 cocultured with *F. nucleatum* (**Fig. 2A**), whereas gene set Hallmark_OXPHOS was enriched in *F. nucleatum* (-) control group (Supplementary Fig. S2A), implying that *F. nucleatum* colonization could promote glycolysis and repress oxidative phosphorylation (OXPHOS) simultaneously. Given

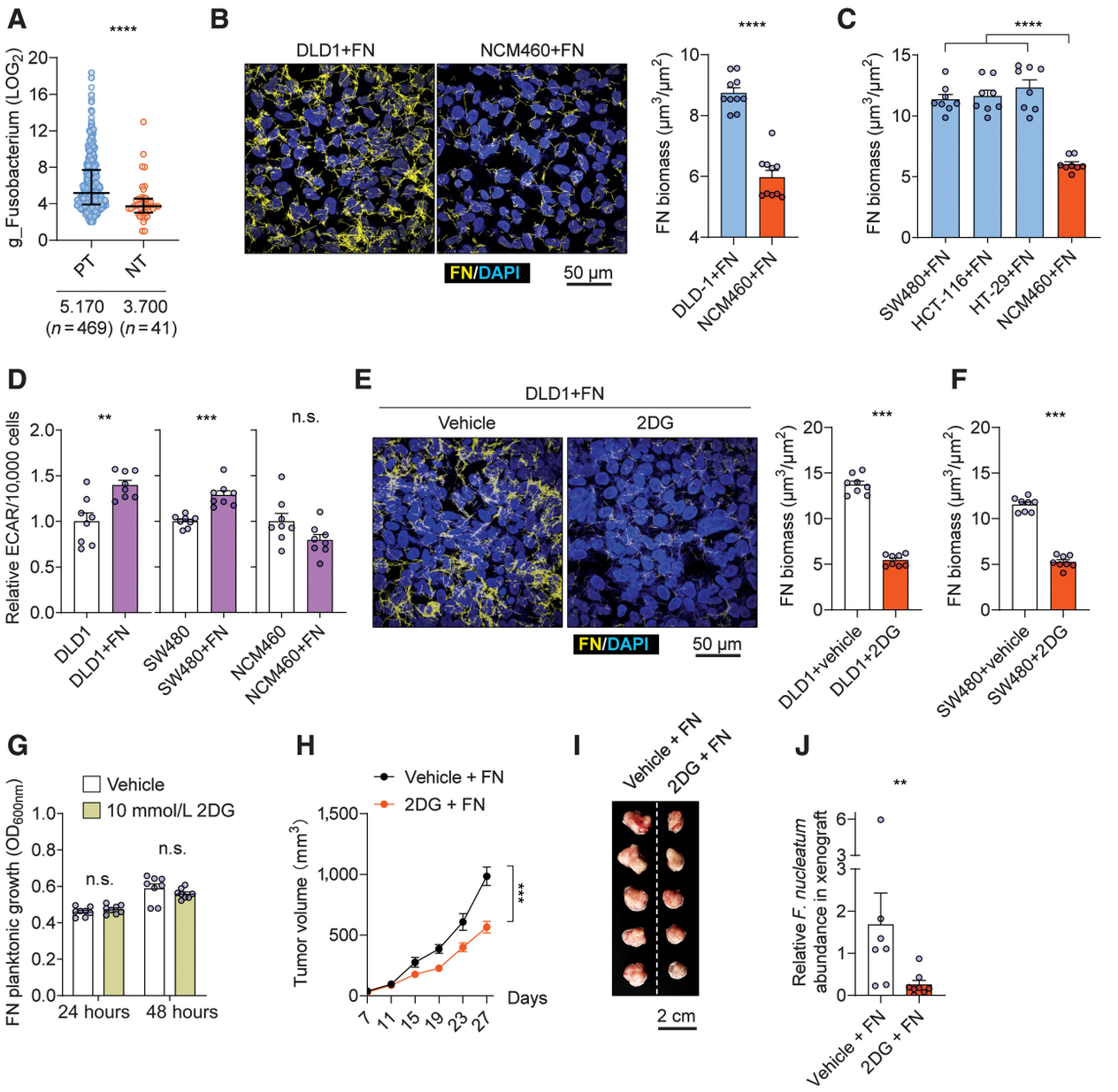

Figure 1.

Enrichment of *F. nucleatum* in colorectal cancer cells is related to enhanced glycolysis. **A,** Abundance of *Fusobacterium* genus (g_Fusobacterium) calculated with RNA-seq data was derived from TCGA-COAD cohort. The median and sample size are shown below each dataset. NT, tumor-adjacent normal tissue; PT, primary tumor. **B,** Representative images and quantification of *F. nucleatum* (FN) stained with FISH in coculture with DLD1 or NCM460. Human cell nuclei were stained with DAPI. $n = 10$ samples. **C,** Quantification of *F. nucleatum* stained with FISH in coculture with different colorectal cancer cell lines or NCM460. $n = 8$ samples. **D,** Relative ECAR of different cell lines cultured with or without *F. nucleatum*. $n = 8$ samples. **E** and **F,** Quantification of stained *F. nucleatum* biomass in coculture with DLD1 (**E**) or SW480 (**F**), with or without treatment of 2DG (10 mmol/L). $n = 8$ samples. Representative images of stained *F. nucleatum* and DLD1 cocultures are shown in **E**. **G,** Planktonic growth of *F. nucleatum* measured by OD_{600nm} under the treatment of vehicle or 2DG. $n = 8$ samples. **H,** Xenograft tumor volume under different conditions. Mice were treated with *F. nucleatum* and with PBS vehicle ($n = 7$) or 2DG ($n = 8$). **I,** Representative images of tumors under different conditions. **J,** Relative *F. nucleatum* abundance in xenograft tumors quantified with qPCR. The data in **A** are presented as median with interquartile range, and the data in **B**–**H** and **J** are presented as mean ± SEM. Each circle represents an individual sample. Samples were collected from three independent experiments in **B**–**G** and from two independent experiments in **H**–**J** (n.s., nonsignificant, $P < 0.05$; **, $P < 0.01$; ***, $P < 0.001$; ****, $P < 0.0001$ by Wilcoxon rank-sum test or Welch ANOVA test for single or grouped analyses, respectively).

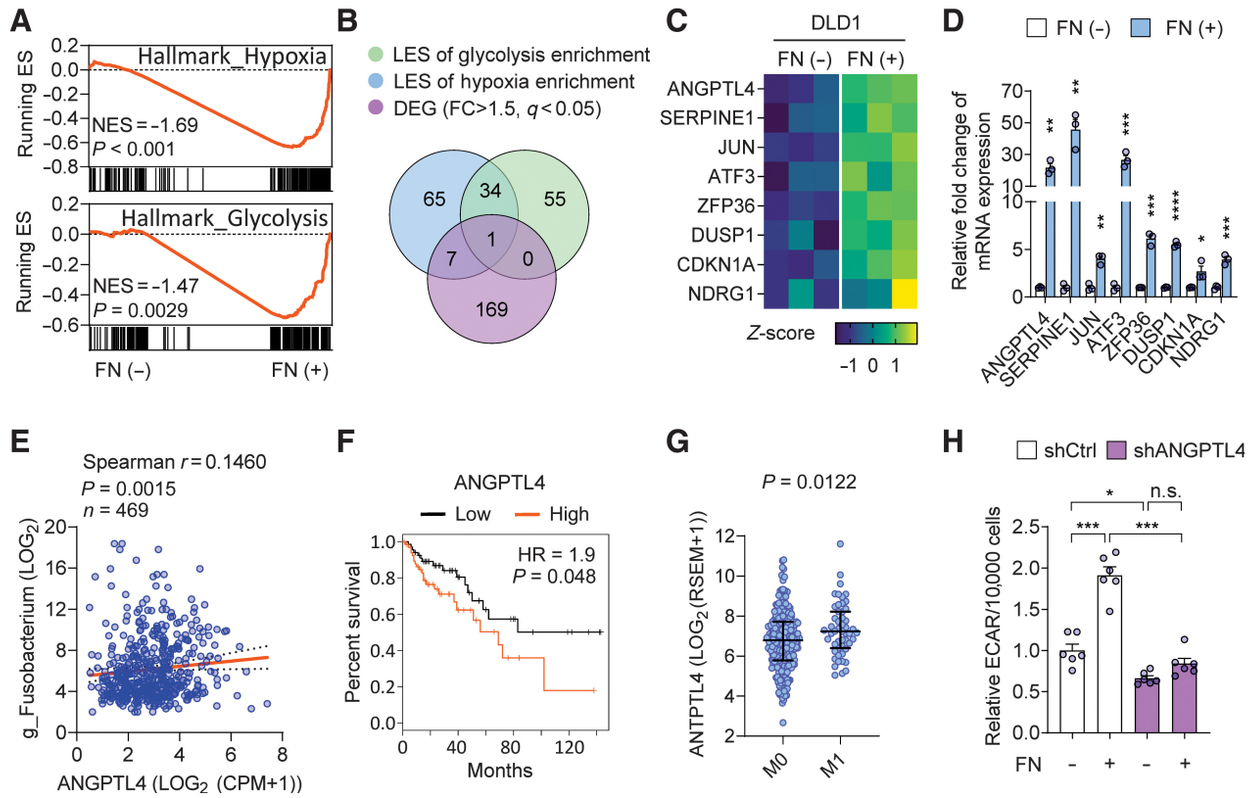

Figure 2.

F. nucleatum promotes glycolysis via inducing ANGPTL4 expression in colorectal cancer cells. **A,** GSEA of RNA-seq data compared the transcriptome of DLD1 cultured with or without *F. nucleatum* (FN). ES, enrichment score; NES, net enrichment score. $n = 3$ samples. **B,** Selection of the DEGs between FN (−) and FN (+) groups that were also related to the enrichment of gene sets of Hallmark_Hypoxia and/or Hallmark_Glycolysis. Numbers of overlapped genes are indicated. FC, fold change; *q*, adjusted *P* value. **C,** Heatmap for DEGs selected in **B**. $n = 3$ samples. **D,** qPCR analysis of the selected DEGs in DLD1 cultured with or without *F. nucleatum*. $n = 3$ samples. **E,** Spearman correlation between the abundance of *Fusobacterium* genus (g_Fusobacterium) and expression level of ANGPTL4 in primary tumor tissues ($n = 469$) of TCGA-COAD patients. Data were acquired from TCGA database and Poore and colleague's study (21). The orange line represents the best-fit linear regression, and the dotted line represents the 95% confidence intervals. **F,** Overall survival plots of patients with high ($n = 68$) and low ($n = 68$) ANGPTL4 expression levels (quartile group cutoff) analyzed in the GEPIA database. Log-rank test. HR, hazard ratio. **G,** Expression level of ANGPTL4 in primary tumor tissues of TCGA-COAD patients with (M1, $n = 255$) or without (M0, $n = 51$) metastasis. **H,** Relative ECAR of DLD1 cultured with or without *F. nucleatum*. Cells were transfected with lentivirus-delivered nontarget shRNA control (shCtrl) or ANGPTL4-target shRNA (shANGPTL4). $n = 6$ samples. The data in **D** and **H** are presented as mean ± SEM, and the data in **G** are presented as median with interquartile range. Each circle represents an individual sample in **D**, **E**, **G**, and **H**. Samples were collected from three independent experiments in **D** and **H** (n.s., nonsignificant, $P < 0.05$; *, $P < 0.01$; **, $P < 0.01$; ***, $P < 0.001$; ****, $P < 0.0001$ by Wilcoxon rank-sum test or Welch ANOVA test for single or grouped analyses, respectively).

the frequent concurrence of hypoxia and glycolysis (29), we evaluated the overlap of DEG with the leading-edge subgroup (LES) of genes responsible for the enrichment of Hallmark_Hypoxia or Hallmark_Glycolysis. Among eight overlapped genes, the gene encoding for angiopoietin-like protein 4 (ANGPTL4), which is significantly upregulated in *F. nucleatum* (+) group, was the only one contributed to the enrichment of both gene sets related to hypoxia and glycolysis (**Fig. 2B** and **C**). The other seven genes including *SERPINE1*, *JUN*, *ATF3*, and so on were related to hypoxia (**Fig. 2B** and **C**). The *F. nucleatum*–induced upregulation of these genes was confirmed by qPCR in DLD1, SW480, and HCT-116 (**Fig. 2D**; Supplementary Fig. S2B and S2C). Coculture with *F. nucleatum* also enhanced the expression of ANGPTL4 and SERPINE1 in NCM460, but to a much lesser extent compared with that in colorectal cancer cells (Supplementary Fig. S2D).

By analyzing the transcriptome data derived from the TCGA-COAD cohort, a significant positive correlation between the expression level of ANGPTL4 and the abundance of *Fusobacterium* genus in primary tumor tissues was demonstrated (**Fig. 2E**). Moreover, high level of ANGPTL4 expression was associated with the shortened survival of patients with COAD (**Fig. 2F**). Primary tumor tissues derived from patient with COAD with metastasis exhibited higher expression level of ANGPTL4 than nonmetastatic ones (**Fig. 2G**).

Further investigations into the influence of ANGPTL4 on glycolysis revealed that overexpression of the gene promoted ECAR in DLD1, whereas knockdown of this gene exhibited a mild inhibitory effect against glycolysis (Supplementary Fig. S2E and S2H). More importantly, knockdown of ANGPTL4 in DLD1 abrogated the glycolysis promoting effect of *F. nucleatum* (**Fig. 2H**).

ANGPTL4 is required for the colonization of *F. nucleatum* in colorectal cancer cells

As *F. nucleatum* colonization could promote glycolysis of colorectal cancer cells, at least in part by upregulation ANGPTL4 expression, and meanwhile glycolysis activity was related with *F. nucleatum* colonization both *in vitro* and *in vivo*, we reasoned that *F. nucleatum* could

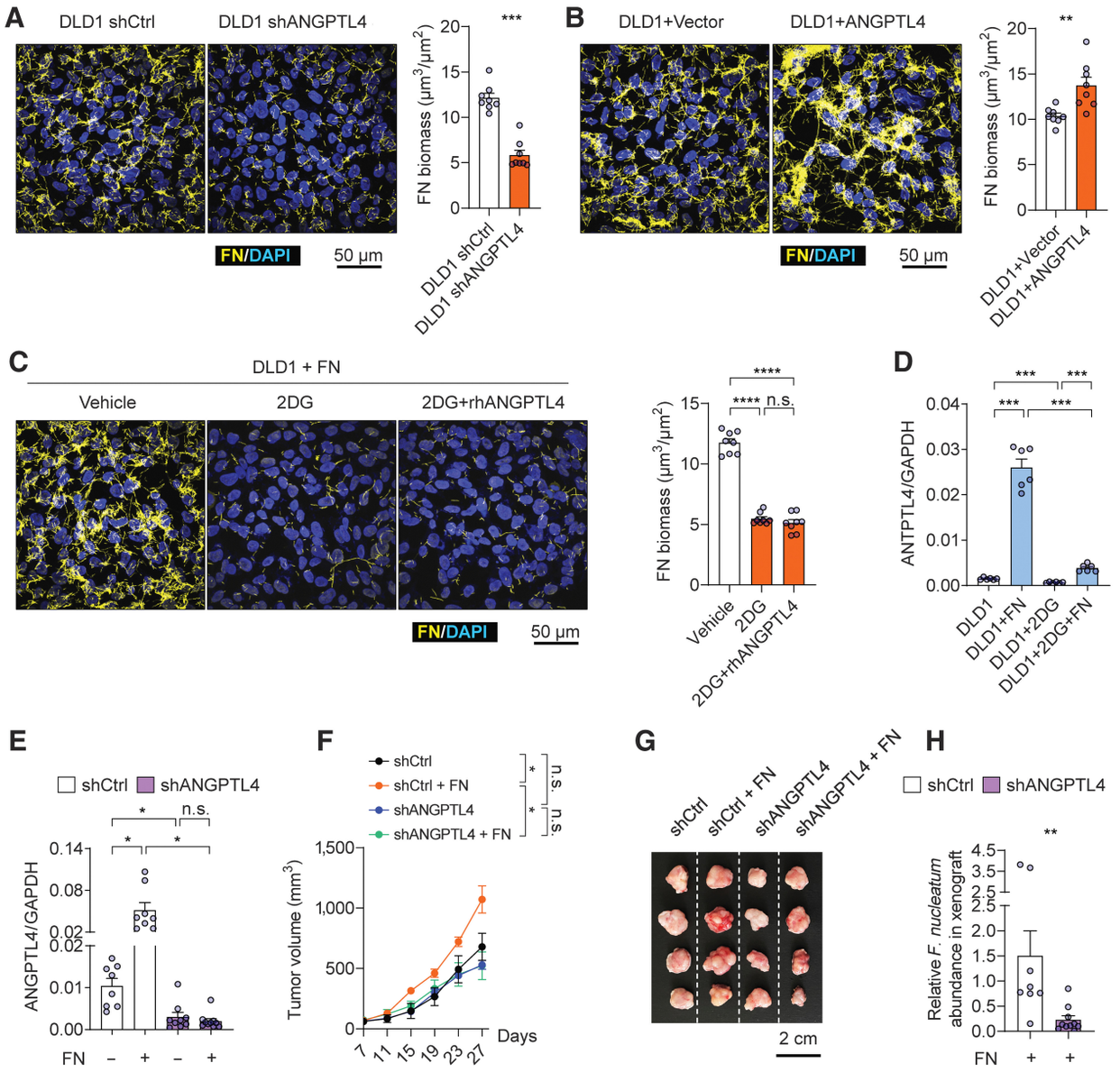

Figure 3.

The colonization of *F. nucleatum* in colorectal cancer cells depends on ANGPTL4. **A–C,** Representative images and quantification of *F. nucleatum* (FN) stained with FISH in coculture with DLD1. The impact of ANGPTL4 knockdown (**A**), ANGPTL4 overexpression (**B**), or treatment with 2DG (10 mmol/L)/rhANGPTL4 (5 μg/mL; **C**) on *F. nucleatum* colonization in cocultures was evaluated. $n = 8$ samples. **D,** qPCR measurement of ANGPTL4 mRNA level in DLD1 cultured with or without *F. nucleatum*, treated with or without 2DG (10 mmol/L; $n = 6$ samples). **E,** ANGPTL4 expression level in xenograft tumors under different conditions. Mice were treated with AAV-delivered shRNA for nontarget control (shCtrl) or ANGPTL4 knockdown (shANGPTL4), and with or without *F. nucleatum*. $n = 8$ for shCtrl and shCtrl + FN group; $n = 9$ for shANGPTL4 group; and $n = 10$ for shANGPTL4 + FN group. **F,** Xenograft tumor volume under different conditions. **G,** Representative images of tumors under different conditions. **H,** Relative *F. nucleatum* abundance in xenograft tumors quantified with qPCR. The data are presented as mean ± SEM. Each circle represents an individual sample. Samples were collected from three independent experiments in **A–D** and from two independent experiments in **E–H** (n.s., nonsignificant, $P < 0.05$; *, $P < 0.05$; **, $P < 0.01$; ***, $P < 0.001$; ****, $P < 0.0001$ by Wilcoxon rank-sum test or Welch ANOVA test for single or grouped analyses, respectively).

induce ANGPTL4 expression and consequently favor its colonization and growth in colorectal cancer cells and tumor tissues. To support this hypothesis, we found that shRNA knockdown of ANGPTL4 in DLD1 could remarkably repress the overall biomass of *F. nucleatum* (**Fig. 3A**). Moreover, overexpression of ANGPTL4 and exogenous addition of recombinant human ANGPTL4 (rhANGPTL4) in the culture of DLD1 further promoted *F. nucleatum* colonization (**Fig. 3B**; Supplementary Fig. S3). Of note, the inhibitory effect of 2DG on *F. nucleatum* colonization could not be rescued by treatment of rhANGPTL4 (**Fig. 3C**), and the *F. nucleatum*–induced increase of ANGPTL4 expression in DLD1 could also be diminished by 2DG treatment (**Fig. 3D**), suggesting that enhanced glycolysis activity was necessary for *F. nucleatum* colonization in colorectal cancer cells promoted by ANGPTL4. Although SERPINE1 was also remarkably

upregulated by *F. nucleatum* infection, the knockdown of the gene had no effect on *F. nucleatum* colonization in DLD1 or SW480 (Supplementary Fig. S4). The *F. nucleatum*–induced ANGPTL4 expression was confirmed in xenograft-bearing mice (**Fig. 3E**). ANGPTL4 knockdown in xenografts significantly reduced *F. nucleatum* abundance in tumors and meanwhile abolished the promoting effect of *F. nucleatum* toward tumor growth (**Fig. 3F–H**).

ANGPTL4 facilitates *F. nucleatum* colonization by enhancing glucose uptake

It has been previously reported that ANGPTL4 promoted cellular bioenergetics in multiple cancer cell lines and associated xenograft models (30, 31). Exogenous recombinant C-terminal form of ANGPTL4 has been identified to enhance GLUT1 expression and glucose uptake (30, 31). GLUT1 was the most highly expressed glucose transporters in DLD1 (**Fig. 4A**). Coculture with *F. nucleatum* upregulated both ANGPTL4 and GLUT1 in DLD1 and SW480 (**Fig. 4B**; Supplementary Fig. S5A), whereas had no such effects in NCM460 (Supplementary Fig. S5A). The data from TCGA-COAD cohort confirmed a positive correlation between mRNA levels of ANGPTL4 and GLUT1 in primary tumor tissues (**Fig. 4C**). In line with the elevated expression of GLUT1, *F. nucleatum* colonized DLD1 exhibited increased ability for glucose uptake (**Fig. 4D**). As expected, overexpression of ANGPTL4 elevated the mRNA and protein level of GLUT1 and promoted glucose uptake in DLD1 and SW480 (**Fig. 4E–G**; Supplementary Fig. S5B), whereas its knockdown exhibited opposite impacts (**Fig. 4H–J**; Supplementary Fig. S5B). Consistently, treatment of a GLUT1 inhibitor BAY-876 (32) significantly suppressed *F. nucleatum* colonization in DLD1 and SW480, which could not be rescued by supplementary rhANGPTL4 (**Fig. 4K**; Supplementary Fig. S5C and S5D). *F. nucleatum*–induced upregulation of ANGPTL4 was also diminished by BAY-876 treatment, which might be a consequent of reduced *F. nucleatum* colonization (**Fig. 4L**; Supplementary Fig. S5E). These findings suggested that ANGPTL4, whose expression was increased upon *F. nucleatum* colonization, could in turn facilitated *F. nucleatum* colonization via upregulating GLUT1 expression and glucose uptake.

F. nucleatum promotes ANGPTL4 expression by facilitating the H3K27ac

Previous studies have revealed that transcription factors such like PPARβ/δ and HIF1α, alone with the enhancer marker H3K27ac, were involved in the transcription regulation of ANGPTL4 (33, 34). As the enrichment of hypoxia-related gene set in DLD1 cocultured with *F. nucleatum* had been identified (**Fig. 2A**), we further performed ChIP-qPCR to evaluate the effect of *F. nucleatum* colonization on HIF1α binding as well as H3K27ac level at previously reported sites within ANGPTL4 locus. The results showed that *F. nucleatum* colonization promoted the binding of HIF1α with ANGPTL4 and the level of H3K27ac at its promoter region (**Fig. 5A**). In addition, cocultured with *F. nucleatum* dramatically increased the overall H3K27ac in colorectal cancer cells, which could be abolished due to bacteria elimination by antibiotics treatment (**Fig. 5B–D**). However, another oral anaerobe *P. gingivalis*, which has been claimed to be correlated with certain cancers apart from being a well-documented periodontitis-related pathogen (35, 36), did not have the similar impact on H3K27ac level (**Fig. 5E**). Moreover, *F. nucleatum* exerted a dose-dependent effect on the overall H3K27ac level in DLD1 (**Fig. 5F**) but could not increase H3K27ac in NCM460 even at the highest inoculum (**Fig. 5F** and **G**). The positive correlation between *F. nucleatum* abundance and H3K27ac level was further confirmed in clinical samples of colonic adenocarcinoma (**Fig. 5H** and **I**).

H3K27ac is acetylated mainly by CBP/p300 (37). Treatment of A-485, a selective CBP/p300 inhibitor (38), reduced the overall H3K27ac in DLD1 or SW480 cocultured with *F. nucleatum* to a similar level in *F. nucleatum*–free control, and consistently inhibited the upregulation of ANGPTL4 induced by *F. nucleatum* (**Fig. 6A–D**). Moreover, treatment of A-485 repressed the binding of HIF1α to ANGPTL4 (**Fig. 6E**) and decreased the amount of *F. nucleatum* in cocultures with DLD1 (**Fig. 6F**), which could be rescued by the addition of rhANGPTL4 (**Fig. 6F**). In addition, *F. nucleatum*-induced upregulation of ANGPTL4, GLUT1, and glucose uptake was largely abolished by A-485 treatment (**Fig. 6G–I**). The inhibition of H3K27ac by A-485 treatment did not affect *F. nucleatum*–induced ATF3 expression in both DLD1 and SW480 (Supplementary Fig. S6). In line with our previous identifications that blocking of either glycolysis activity or GLUT1 function eliminated *F. nucleatum* colonization, 2DG or BAY-876 treatment also repressed elevation of H3K27ac level induced by *F. nucleatum* (**Fig. 6J** and **K**). These results indicated that ANGPTL4 expression promoted by *F. nucleatum* in colorectal cancer cells depended on H3K27ac modification.

The knockdown of HIF1A in DLD1 (Supplementary Fig. S7A) did not impact the H3K27ac level within the promoter region of ANGPTL4 (Supplementary Fig. S7B) and had no effect on ANGPTL4 expression in DLD1 cultured without *F. nucleatum* (Supplementary Fig. S7C). Nonetheless, knockdown of HIF1A abrogated the *F. nucleatum*–induced ANGPTL4 expression (Supplementary Fig. S7C), as well as repressed the *F. nucleatum* colonization (Supplementary Fig. S7D).

HDAC activity is suppressed in colorectal cancer cells cocultured with *F. nucleatum*

Given the fact that histone acetylation is under tight regulation of HDACs, which could be modulated by bacterial infection (39), we further determined the impact of *F. nucleatum* colonization on the overall HDAC activity in DLD1. When measured *in situ*, HDAC activity of DLD1 cocultured with *F. nucleatum* was significantly inhibited (**Fig. 7A**). Meanwhile, NCM460 cocultured with *F. nucleatum* exhibited a higher HDAC activity compared with NCM460 cultured alone (**Fig. 7A**). To exclude the influence of *F. nucleatum* itself on the measurement of HDAC activity, nuclear extracts of cells cultured alone or cocultured with *F. nucleatum*/*P. gingivalis* were subsequently tested. The data showed that coculture with *F. nucleatum* instead of *P. gingivalis* could repress HDAC activity in DLD1, but not in NCM460 (**Fig. 7B**). In addition, the alterations of H3K27ac levels in the nuclear extracts corresponded with their HDAC activities, where a lower HDAC activity produced a higher level of H3K27ac (**Fig. 7C** and **D**).

As revealed by DLD1 RNA-seq data, HDAC1–3 exhibited the highest expression levels among all HDACs (**Fig. 7E**). Data derived from TCGA-COAD cohort showed that the abundance of *Fusobacterium* genus was negatively correlated with the expression levels of HDAC1 and HDAC2 (**Fig. 7F**). Consistently, in our in vitro model *F. nucleatum* infection resulted in mild declines in mRNA and protein levels of HDAC1 and HDAC2 in DLD1 and SW480 (**Fig. 7G** and **H**; Supplementary Fig. S8A and S8B), but had no impact on the expression of HDAC1–3 in NCM460 (Supplementary Fig. S8C and S8D). Moreover, conditioned medium from DLD1 infected with *F. nucleatum* (DF-CM) inhibited the activities of recombinant HDAC1 and HDAC2 compared with conditioned medium from DLD1 cultured alone (D-CM), whereas *P. gingivalis*–conditioned medium from DLD1

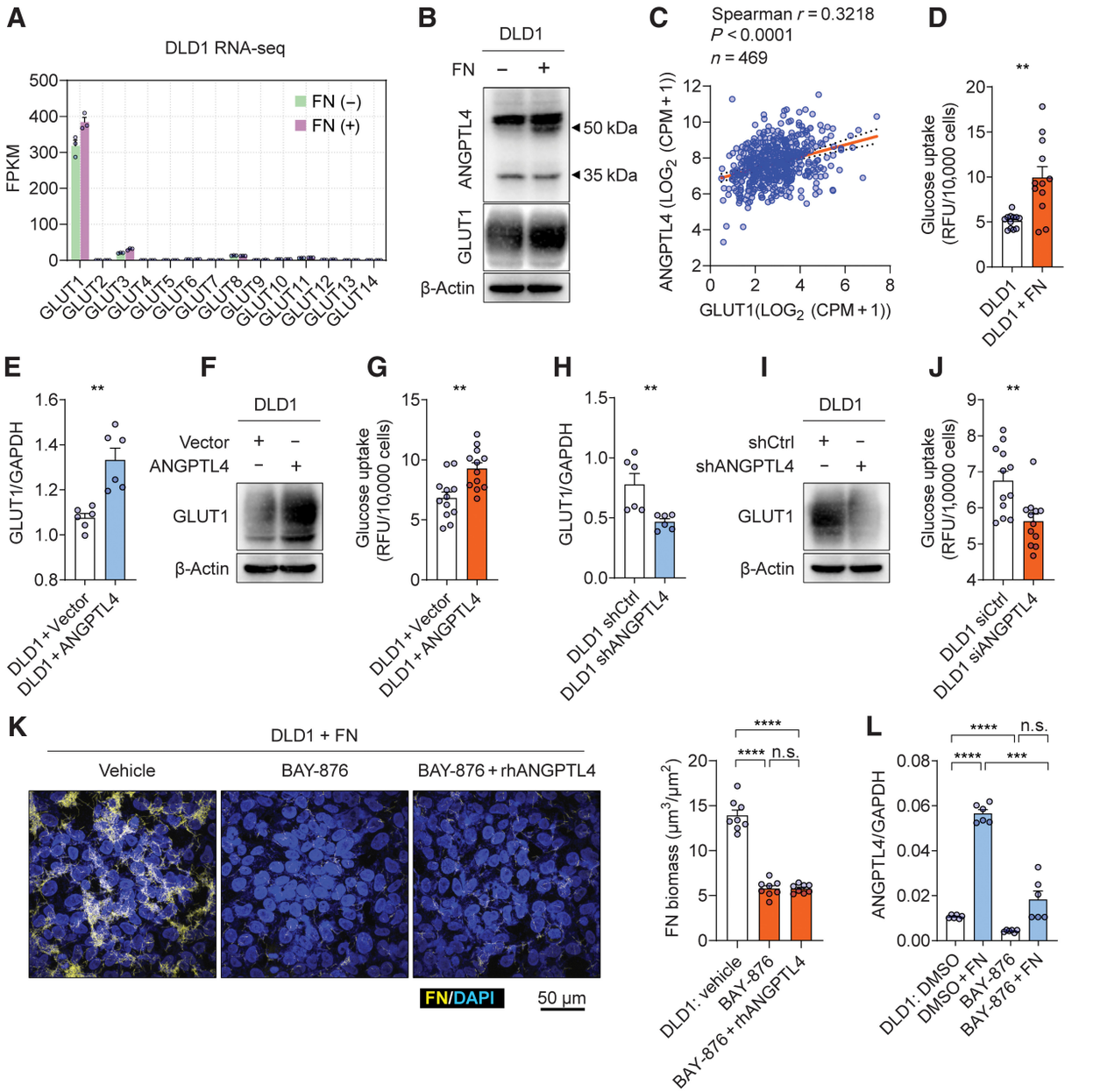

Figure 4.

ANGPTL4 facilitates *F. nucleatum* colonization by enhancing glucose uptake. **A,** mRNA levels of genes encoding glucose transporter (GLUT) 1–14 revealed by the RNA-seq data ($n = 3$ samples). FN, *F. nucleatum*. **B,** Western blot analysis of ANGPTL4 and GLUT1 in DLD1 cultured with or without *F. nucleatum*. The bands of ANGPTL4 in the top panel were observed at 35 and 50 kDa according to the manufacturer's instruction. **C,** Spearman correlation between expression levels of ANGPTL4 and GLUT1 in the primary tumor tissues ($n = 469$). Data were derived from TCGA-COAD cohort. The orange line represents the best-fit linear regression, and the dotted line represents the 95% confidence intervals. **D,** Glucose uptake of DLD1 cultured with or without *F. nucleatum* determined by 2-NBDG fluorescent signals. $n = 12$ samples. **E–G,** The impact of ANGPTL4 overexpression on GLUT1 mRNA level (**E**; $n = 6$ samples), protein level (**F**), and glucose uptake (**G**; $n = 12$ samples) of DLD1. **H–J,** The impact of ANGPTL4 knockdown on GLUT1 mRNA level (**H**; $n = 6$ samples), protein level (**I**), and glucose uptake (**J**; $n = 12$ samples) of DLD1. **K,** Representative images and quantification of FISH-stained *F. nucleatum* in coculture with DLD1, under the treatment of DMSO vehicle, BAY-876 (2 μmol/L), or BAY-876 (2 μmol/L) + rhANGPTL4 (5 μg/mL). Human cell nuclei were stained with DAPI ($n = 8$ samples). **L,** qPCR measurement of ANGPTL4 mRNA level in DLD1 cultured with or without *F. nucleatum*, treated with or without BAY-876 (2 μmol/L; $n = 6$ samples). The data are presented as mean ± SEM. Each circle represents an individual sample. Samples were collected from three independent experiments in **D**, **E**, **G**, **H**, and **J–L**. For Western blots in **B**, **F**, and **I**, two independent experiments were performed with similar results (n.s., nonsignificant, $P < 0.05$; **, $P < 0.01$; ***, $P < 0.001$; ****, $P < 0.0001$ by Wilcoxon rank-sum test or Welch ANOVA test for single or grouped analyses, respectively).

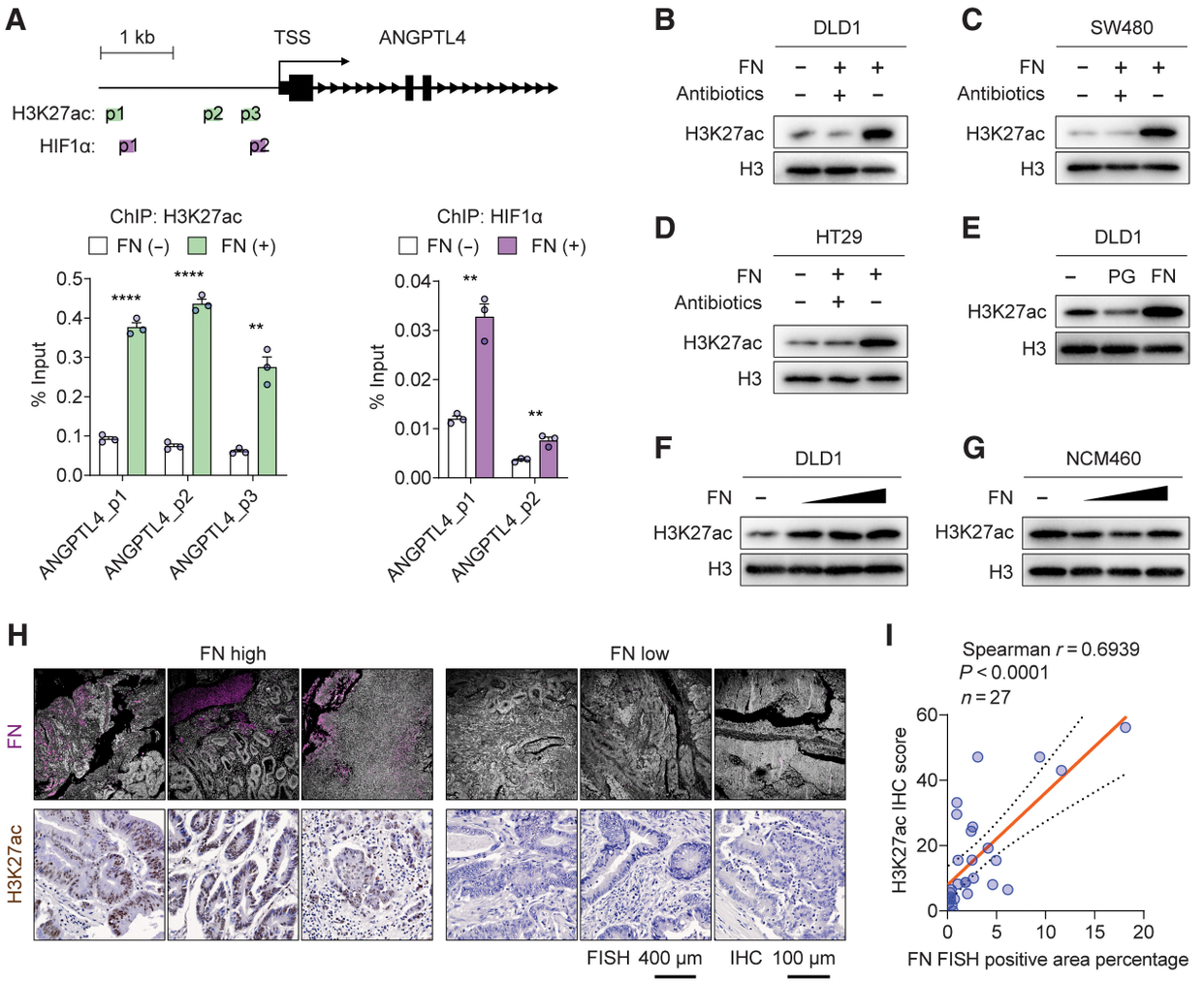

Figure 5.

F. nucleatum colonization enhances the binding of HIF1α with ANGPTL4 and the level of acetylation of H3K27ac. **A,** ChIP-qPCR analysis of the level of H3K27ac and HIF1α binding within the promoter region of ANGPTL4, in DLD1 cultured with or without *F. nucleatum* (FN). Nonspecific DNA immunoprecipitation in isotype IgG control was not detectable (qPCR CT value >45) in all samples. Top, peak regions of H2K27ac and HIF1α binding within ANGPTL4 locus determined with ChIP-seq datasets in Cistrome Data Browser ($n = 3$ samples). TSS, transcription start site. **B–G,** Overall H3K27ac level determined by Western blot in different cell lines with indicated treatment. Gentamicin (300 μg/mL) and metronidazole (200 μg/mL) were added into the cocultures at the same time of *F. nucleatum* inoculation when antibiotics treatment was indicated in **B** and **C**. *F. nucleatum* or *P. gingivalis* (PG) was inoculated at an MOI of 5:1 in **B**–**E** and at an MOI of 5:1, 10:1, or 20:1 in **F** and **G** as indicated. **H,** Representative images of FISH-stained *F. nucleatum* (purple) and IHC-stained H3K27ac (brown) in paraffin-embedded colon adenocarcinoma tissues ($n = 27$). Human cell nuclei were stained with DAPI (gray) in FISH images and with hematoxylin (blue) in IHC images. **I,** Spearman correlation between the H3K27ac IHC score and the percentage of FISH-positive *F. nucleatum* area in paraffin-embedded colon adenocarcinoma tissues ($n = 27$). The orange line represents the best-fit linear regression, and the dotted line represents the 95% confidence intervals. The data in **A** are presented as mean ± SEM. Each circle represents an individual sample in **A** and **I**. Samples were collected from three independent experiments in **A**. For Western blots in **B**–**G**, two independent experiments were performed with similar results (**, $P < 0.01$; ****, $P < 0.0001$ by Wilcoxon rank-sum test).

(DP-CM) or *F. nucleatum*–conditioned medium from NCM460 (NF-CM) had no obvious effects compared with the corresponding control (**Fig. 7I**).

Discussion

The environmental conditions will select for a series of microbial traits that allow the survival and growth of certain microorganism. Previous studies reveal that colorectal cancer tissues or breast cancer cells overexpress a specific sugar residue, Gal-GalNAc, which can be recognized by the fusobacterial adhesin Fap2 (20, 40). Besides, *F. nucleatum* encodes an array of genes related to adhesion and invasion, enabling it to reside intracellularly in host cells (41, 42). However, after localization, microbes need to adapt to the tumor microenvironment to ensure survival. During the adaption, we propose that both *F. nucleatum* and colorectal cancer cells will actively change their behaviors to establish and maintain the symbiotic relationship. Indeed, our results showed coculture with colorectal cancer cells instead of a nonmalignant cell line facilitated the growth of *F. nucleatum*, indicating that inherent properties of tumor cells played

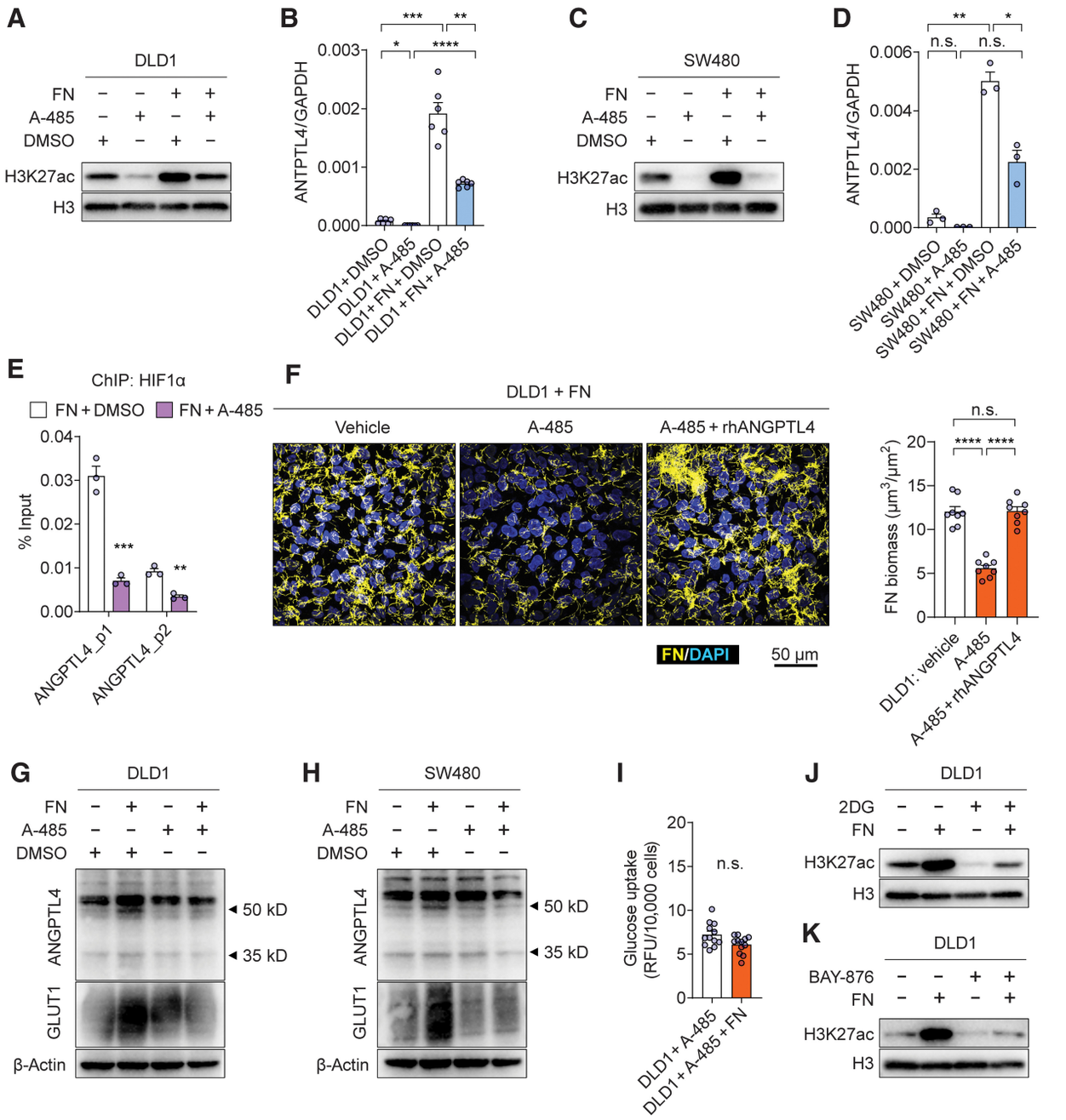

Figure 6.

F. nucleatum–induced ANGPTL4 expression is dependent on H3K27ac. **A–D,** Overall H3K27ac level (**A** and **C**) and ANGPTL4 mRNA (**B** and **D**) quantification in DLD1 (**A** and **B**) or SW480 (**C** and **D**) cultured with or without *F. nucleatum* (FN), treated with DMSO vehicle or A-485 (1 μmol/L; $n = 6$ samples in **B** and $n = 3$ samples in **D**). **E,** ChIP-qPCR analysis of the level of HIF1α binding within the promoter region of ANGPTL4 in DLD1 cocultured with *F. nucleatum* and treated with DMSO vehicle or A-485 (1 μmol/L). Nonspecific DNA immunoprecipitation in isotype IgG control was not detectable (qPCR CT value >45) in all samples ($n = 3$ samples). **F,** Representative images and quantification of FISH-stained *F. nucleatum* in coculture with DLD1, under the treatment of DMSO vehicle, A-485 (1 μmol/L), or A-485 (1 μmol/L) + rhANGPTL4 (5 μg/mL). Human cell nuclei were stained with DAPI ($n = 8$ samples). **G** and **H,** Western blot analysis of ANGPTL4 and GLUT1 in DLD1 (**G**) or SW480 (**H**) cultured with or without *F. nucleatum*, treated with DMSO vehicle or A-485 (1 μmol/L). The bands of ANGPTL4 at the top were observed at 35 and 50 kDa according to the manufacturer's instruction. **I,** The effect of A-485 (1 μmol/L) treatment on glucose uptake of DLD1 cultured with or without *F. nucleatum* determined by 2-NBDG fluorescent signals. $n = 12$ samples. **J** and **K,** Western blot analysis of H3K27ac level in DLD1 cultured with or without *F. nucleatum*, treated with 2DG (10 mmol/L, PBS as vehicle; **J**) or BAY-876 (2 μmol/L, DMSO as vehicle; **K**). The data are presented as mean ± SEM. Each circle represents an individual sample. Samples were collected from three independent experiments in **B**, **D**–**F**, and **I**. For Western blots in **A**, **C**, **G**, **H**, **J**, and **K**, two independent experiments were performed with similar results (n.s., nonsignificant, $P < 0.05$; *, $P < 0.05$; **, $P < 0.01$; ***, $P < 0.001$; ****, $P < 0.0001$ by Wilcoxon rank-sum test or Welch ANOVA test for single or grouped analyses, respectively).

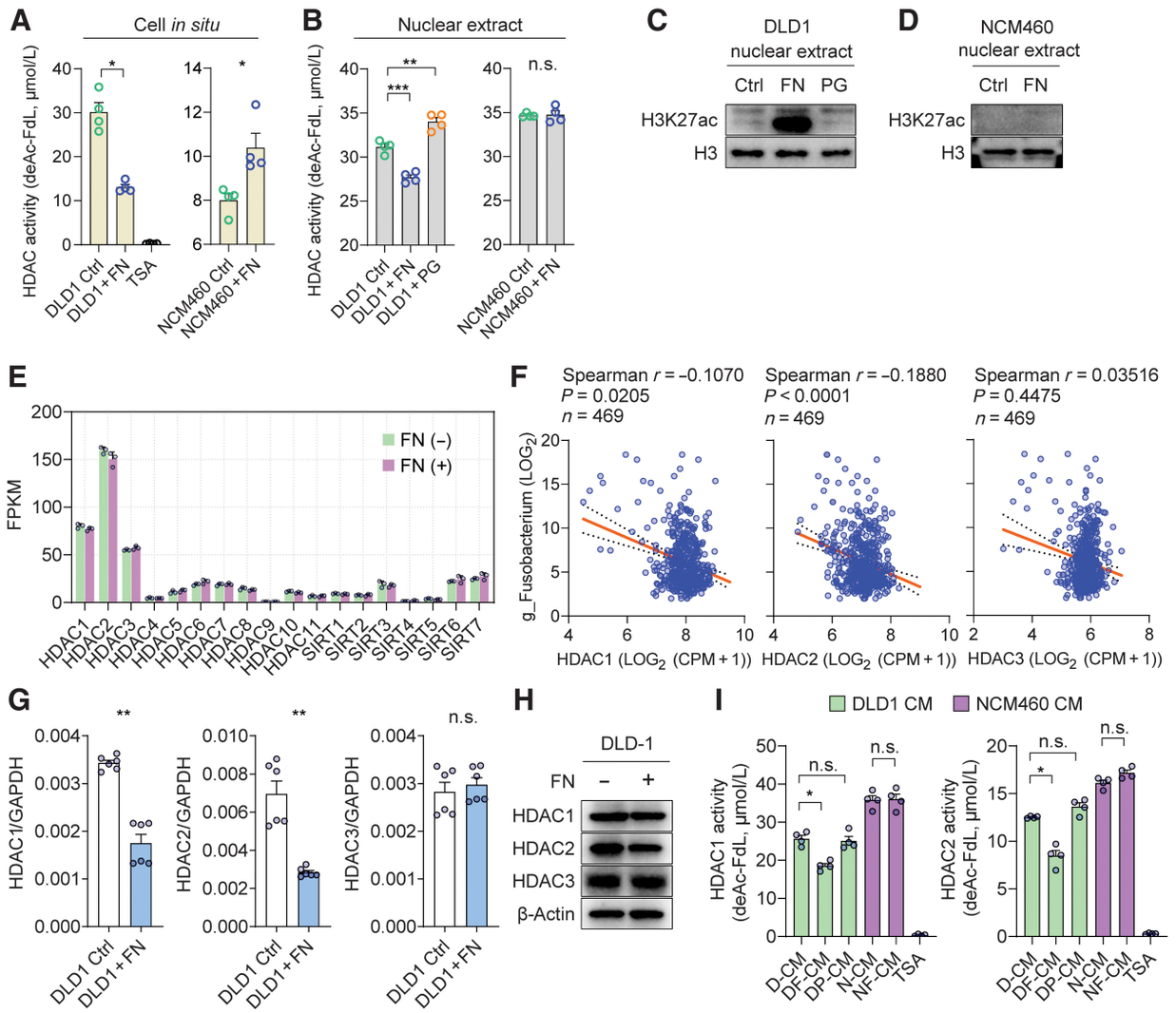

Figure 7.

HDAC activity is suppressed in colorectal cancer cells cocultured with *F. nucleatum*. **A,** *In situ* HDAC activity measured in DLD1 or NCM460 cultured with or without *F. nucleatum* (FN); 1 μmol/L TSA was used as a positive control for HDAC activity inhibition. deAc-FdL, deacetylated FLUOR DE LYS substrate ($n = 4$ samples). **B–D,** Nuclear protein was extracted from DLD1 or NCM460 cultured with or without *F. nucleatum* or *P. gingivalis* (PG). HDAC activity (**B**; $n = 4$ samples) or H3K27ac level (**C** and **D**) was quantified, respectively. **E,** mRNA levels of genes encoding HDAC1–11 and SIRT1–7 revealed by the RNA-seq data ($n = 3$ samples). **F,** Spearman correlation between the abundance of *Fusobacterium* genus (g_Fusobacterium) and the expression level of HDAC1–3 in the primary tumor tissues from TCGA-COAD patients ($n = 469$). The orange line represents the best-fit linear regression, and the dotted line represents the 95% confidence intervals. **G** and **H,** HDAC1–3 mRNA (**G**; $n = 6$ samples) and protein (**H**) levels quantified in DLD1 cultured with or without *F. nucleatum*. **I,** The deacetylation activity of recombinant human HDAC1 or HDAC2 (2 μg per assay well) treated with indicated conditioned medium (CM); 1 μmol/L TSA was used as a positive control for HDAC activity inhibition ($n = 4$ samples). D-CM, CM from DLD1; DF-CM, CM from DLD1 infected with *F. nucleatum*; DP-CM, CM from DLD1 infected with *P. gingivalis*; N-CM, CM from NCM460; NF-CM, CM from NCM460 infected with *F. nucleatum*. The data are presented as mean ± SEM. Each circle represents an individual sample. Samples were collected from two independent experiments in **A**, **B**, and **I**, and from three independent experiments in **G**. For Western blot in **C**, **D**, and **H**, two independent experiments were performed with similar results (n.s., nonsignificant, $P < 0.05$; *, $P < 0.05$; **, $P < 0.01$; ***, $P < 0.001$ by Wilcoxon rank-sum test or Welch ANOVA test for single or grouped analyses, respectively).

a role in the maintenance of symbiosis. Preference of glycolysis over oxidative phosphorylation for glucose catabolism even under aerobic condition is a well-established hallmark of cancer cells, known as the Warburg effect (43). Intriguingly, the proglycolysis effect of *F. nucleatum* infection could only be observed in colorectal cancer cells and blocking of glycolysis abrogated the *F. nucleatum* colonization in colorectal cancer tissues. It can thus be suggested that the enhancing of glycolysis could be a metabolic adaption of colorectal cancer cells to the *F. nucleatum* infection. In turn, the proliferation of the cancer cells maintained a hypoxic microenvironment securing the persistence of the anaerobic bacterium. Indeed, our *in vitro* RNA-seq data indicating that the *F. nucleatum* colonization promoted the enrichment of gene sets related with hypoxia in colorectal cancer cells. Another possible explanation of our finding is that the

intracellular *F. nucleatum* senses the accumulation of certain metabolites due to the metabolic shift from OXPHOS to glycolysis in colorectal cancer cells to acquire antimicrobial resistance, a similar mechanism involved in the interaction between *Salmonella typhimurium* and macrophages revealed by a recent study (44).

A recent study by Hong and colleagues elucidates that *F. nucleatum* activates glycolysis via a selective increase of lncRNA ENO1-IT1, which subsequently upregulates the expression of a key glycolytic enzyme ENO-1 (9). In this study, ANGPTL4 was identified to be another possible upstream regulator of *F. nucleatum*–mediated glycolysis activation in colorectal cancer cells. In accordance with our results, recent studies demonstrates that ANGPTL4 augments cellular metabolic activity and secures ample cellular energy to confer epithelial–mesenchymal transition (EMT)-mediated metastasis and chemoresistance (30, 31). In a gastric carcinoma cell line MKN74, exogenous rh-cANGPTL4 alone elevated 2-NBDG uptake associated with increased GLUT1 protein expression and augmented the energy charge status during EMT (30). Conversely, the immunoneutralization or siRNA knockdown of ANGPTL4 reduced 2-NBDG uptake and diminished glycolysis (30, 31). Intriguingly, our results showed that the *F. nucleatum*-induced ANGPTL4 expression was indispensable for not only the enhancement of glycolysis in colorectal cancer cells, but also for the colonization of *F. nucleatum in vivo* and *in vitro*. It is noteworthy that the ANGPTL4-mediated promotion of glucose uptake of colorectal cancer cells will likely not deprive the metabolic sources for the survival of *F. nucleatum*, which is an asaccharolytic bacterium that can utilize amino acids and peptides as nutrient sources in the tumor microenvironment (45).

Hypoxia is commonly associated with the environment of solid tumors and promotes invasion, metastasis, and malignancy (46). The HIF1α has been shown to directly upregulate ANGPTL4 expression that facilitates transendothelial migration and increases angiogenesis (47). On the basis of our findings, *F. nucleatum* infection induce the enrichment of genes related with hypoxia in DLD1 and promote the binding of HIF1α to the chromatin locus of ANGPTL4, which explained the upregulation of the gene in the coculture. As reported previously, HIF1α–dependent ANGPTL4 transcription was also linked to CBP/p300-mediated H3K27ac, a marker of enhancer (33). Coculture with *F. nucleatum* not only enhanced the intensity of H3K27ac at the HIF1α binding sites within ANGPTL4 locus, but also promoted the overall H3K27ac level in colorectal cancer cells. This overall enhancement of H3K27ac could be attributed to the repressed HDAC activity in the coculture with *F. nucleatum* as revealed by our *in vitro* assay. Meanwhile, in the coculture of *F. nucleatum* and NCM460, or of *P. gingivalis* and DLD1, the inhibition of HDACs was not observed, suggesting that the colonization and persistence of *F. nucleatum* was prerequisite for such an effect. It is likely that HDAC activity was repressed by the accumulation of lactate derived from the promoted glycolysis of colorectal cancer cells in the coculture (39, 48), or by the well-known HDAC inhibitor butyrate, which could be generated by *F. nucleatum* (49, 50). However, the mechanism underlies the HDAC repression in the coculture needs further clarification. Notwithstanding, we demonstrated here that H3K27ac was indispensable for the induction of ANGPTL4 expression and its downstream effects such as promoting glucose uptake and *F. nucleatum* colonization in the coculture.

In conclusion, this study shows that *F. nucleatum* promotes glycolysis in colorectal cancer cells via induction of ANGPTL4, which could in turn facilitate the persistence of the bacterium itself. Our findings clearly suggest that a microbe could actively modulate the behaviors of cancer cells to define a microenvironment favoring its own survival, thus establishing a symbiosis between the microorganisms and host cells. Interfering with the symbiosis between *F. nucleatum* and cancer cells could be a targeted approach that provides an alternative to using nonspecific antibiotics in clinical treatment of colorectal cancer with *F. nucleatum* infection.

Authors' Disclosures

X. Zheng reports grants from National Natural Science Foundation of China and China Postdoctoral Science Foundation during the conduct of the study. No disclosures were reported by the other authors.

Authors' Contributions

X. Zheng: Conceptualization, resources, data curation, software, formal analysis, funding acquisition, validation, investigation, visualization, methodology, writing–original draft. **R. Liu:** Resources, data curation, formal analysis, validation, investigation, methodology, writing–original draft. **C. Zhou:** Data curation, formal analysis, validation, investigation, methodology. **H. Yu:** Data curation, software, formal analysis, validation, investigation, visualization, methodology. **W. Luo:** Resources, investigation. **J. Zhu:** Investigation, methodology. **J. Liu:** Software, investigation, methodology. **Z. Zhang:** Resources, methodology. **N. Xie:** Resources, methodology. **X. Peng:** Resources, data curation, methodology. **X. Xu:** Data curation, methodology. **L. Cheng:** Data curation, methodology. **Q. Yuan:** Conceptualization, writing–review and editing. **C. Huang:** Conceptualization, resources, supervision, project administration, writing–review and editing. **X. Zhou:** Conceptualization, resources, supervision, funding acquisition, project administration, writing–review and editing.

Acknowledgments

This work was supported by the National Natural Science Foundation of China (81900995 to X. Zheng; 81821002 to C. Huang), the China Postdoctoral Science Foundation (2020M673266 to X. Zheng), the Research Funding for Talents Developing, West China Hospital of Stomatology Sichuan University (RCDWJS2020-11 to X. Zheng), and the Open Fund of the State Key Laboratory of Oral Diseases, Sichuan University (SKLOD202101 to X. Zhou).

The publication costs of this article were defrayed in part by the payment of publication fees. Therefore, and solely to indicate this fact, this article is hereby marked "advertisement" in accordance with 18 USC section 1734.

Note

Supplementary data for this article are available at Cancer Research Online (http://cancerres.aacrjournals.org/).

Received July 13, 2021; revised September 12, 2021; accepted October 11, 2021; published first October 13, 2021.

References

1. Siegel RL, Miller KD, Goding Sauer A, Fedewa SA, Butterly LF, Anderson JC, et al. Colorectal cancer statistics, 2020. CA Cancer J Clin 2020;70:145–64.
2. Janney A, Powrie F, Mann EH. Host-microbiota maladaptation in colorectal cancer. Nature 2020;585:509–17.
3. Castellarin M, Warren RL, Freeman JD, Dreolini L, Krzywinski M, Strauss J, et al. Fusobacterium nucleatum infection is prevalent in human colorectal carcinoma. Genome Res 2012;22:299–306.
4. Kostic AD, Gevers D, Pedamallu CS, Michaud M, Duke F, Earl AM, et al. Genomic analysis identifies association of Fusobacterium with colorectal carcinoma. Genome Res 2012;22:292–8.
5. Mima K, Nishihara R, Qian ZR, Cao Y, Sukawa Y, Nowak JA, et al. Fusobacterium nucleatum in colorectal carcinoma tissue and patient prognosis. Gut 2016;65:1973–80.
6. Tahara T, Yamamoto E, Suzuki H, Maruyama R, Chung W, Garriga J, et al. Fusobacterium in colonic flora and molecular features of colorectal carcinoma. Cancer Res 2014;74:1311–8.
7. Yachida S, Mizutani S, Shiroma H, Shiba S, Nakajima T, Sakamoto T, et al. Metagenomic and metabolomic analyses reveal distinct stage-specific phenotypes of the gut microbiota in colorectal cancer. Nat Med 2019;25:968–76.

8. Hajishengallis G. Periodontitis: from microbial immune subversion to systemic inflammation. Nat Rev Immunol 2015;15:30–44.
9. Hong J, Guo F, Lu SY, Shen C, Ma D, Zhang X, et al. F. nucleatum targets lncRNA ENO1-IT1 to promote glycolysis and oncogenesis in colorectal cancer. Gut 2021; 70:2123–37.
10. Kostic AD, Chun E, Robertson L, Glickman JN, Gallini CA, Michaud M, et al. Fusobacterium nucleatum potentiates intestinal tumorigenesis and modulates the tumor-immune microenvironment. Cell Host Microbe 2013;14:207–15.
11. Rubinstein MR, Wang X, Liu W, Hao Y, Cai G, Han YW. Fusobacterium nucleatum promotes colorectal carcinogenesis by modulating E-cadherin/beta-catenin signaling via its FadA adhesin. Cell Host Microbe 2013;14:195–206.
12. Yang Y, Weng W, Peng J, Hong L, Yang L, Toiyama Y, et al. Fusobacterium nucleatum increases proliferation of colorectal cancer cells and tumor development in mice by activating toll-like receptor 4 signaling to nuclear factor-kappaB, and up-regulating expression of MicroRNA-21. Gastroenterology 2017; 152:851–66.
13. Casasanta MA, Yoo CC, Udayasuryan B, Sanders BE, Umana A, Zhang Y, et al. Fusobacterium nucleatum host-cell binding and invasion induces IL-8 and CXCL1 secretion that drives colorectal cancer cell migration. Sci Signal 2020; 13:eaba9157.
14. Chen S, Su T, Zhang Y, Lee A, He J, Ge Q, et al. Fusobacterium nucleatum promotes colorectal cancer metastasis by modulating KRT7-AS/KRT7. Gut Microbes 2020;11:511–25.
15. Chen Y, Zhang J, Cao P, Su W, Deng Y, Zhan N, et al. Fusobacterium nucleatum promotes metastasis in colorectal cancer by activating autophagy signaling via the upregulation of CARD3 expression. Theranostics 2020;10:323–39.
16. Guo S, Chen J, Chen F, Zeng Q, Liu WL, Zhang G. Exosomes derived from Fusobacterium nucleatum-infected colorectal cancer cells facilitate tumour metastasis by selectively carrying miR-1246/92b-3p/27a-3p and CXCL16. Gut 2020.
17. Yu T, Guo F, Yu Y, Sun T, Ma D, Han J, et al. Fusobacterium nucleatum promotes chemoresistance to colorectal cancer by modulating autophagy. Cell 2017;170: 548–63.
18. Zhang S, Yang Y, Weng W, Guo B, Cai G, Ma Y, et al. Fusobacterium nucleatum promotes chemoresistance to 5-fluorouracil by upregulation of BIRC3 expression in colorectal cancer. J Exp Clin Cancer Res 2019;38:14.
19. Bullman S, Pedamallu CS, Sicinska E, Clancy TE, Zhang X, Cai D, et al. Analysis of Fusobacterium persistence and antibiotic response in colorectal cancer. Science 2017;358:1443–8.
20. Abed J, Emgard JE, Zamir G, Faroja M, Almogy G, Grenov A, et al. Fap2 mediates Fusobacterium nucleatum colorectal adenocarcinoma enrichment by binding to tumor-expressed Gal-GalNAc. Cell Host Microbe 2016;20:215–25.
21. Poore GD, Kopylova E, Zhu Q, Carpenter C, Fraraccio S, Wandro S, et al. Microbiome analyses of blood and tissues suggest cancer diagnostic approach. Nature 2020;579:567–74.
22. Zheng X, Cheng X, Wang L, Qiu W, Wang S, Zhou Y, et al. Combinatorial effects of arginine and fluoride on oral bacteria. J Dent Res 2015;94:344–53.
23. Valm AM, Mark Welch JL, Rieken CW, Hasegawa Y, Sogin ML, Oldenbourg R, et al. Systems-level analysis of microbial community organization through combinatorial labeling and spectral imaging. Proc Natl Acad Sci U S A 2011; 108:4152–7.
24. Heydorn A, Nielsen AT, Hentzer M, Sternberg C, Givskov M, Ersboll BK, et al. Quantification of biofilm structures by the novel computer program COMSTAT. Microbiology (Read) 2000;146:2395–407.
25. Subramanian A, Tamayo P, Mootha VK, Mukherjee S, Ebert BL, Gillette MA, et al. Gene set enrichment analysis: a knowledge-based approach for interpreting genome-wide expression profiles. Proc Natl Acad Sci U S A 2005;102:15545–50.
26. Padua D, Zhang XH, Wang Q, Nadal C, Gerald WL, Gomis RR, et al. TGFbeta primes breast tumors for lung metastasis seeding through angiopoietin-like 4. Cell 2008;133:66–77.
27. Varghese F, Bukhari AB, Malhotra R, De A. IHC Profiler: an open source plugin for the quantitative evaluation and automated scoring of immunohistochemistry images of human tissue samples. PLoS One 2014;9:e96801.
28. Warburg O. On the origin of cancer cells. Science 1956;123:309–14.
29. Lee P, Chandel NS, Simon MC. Cellular adaptation to hypoxia through hypoxia inducible factors and beyond. Nat Rev Mol Cell Biol 2020;21:268–83.
30. Teo Z, Sng MK, Chan JSK, Lim MMK, Li Y, Li L, et al. Elevation of adenylate energy charge by angiopoietin-like 4 enhances epithelial-mesenchymal transition by inducing 14–3-3gamma expression. Oncogene 2017;36:6408–19.
31. Lim MMK, Wee JWK, Soong JC, Chua D, Tan WR, Lizwan M, et al. Targeting metabolic flexibility via angiopoietin-like 4 protein sensitizes metastatic cancer cells to chemotherapy drugs. Mol Cancer 2018;17:152.
32. Wu Q, Ba-Alawi W, Deblois G, Cruickshank J, Duan S, Lima-Fernandes E, et al. GLUT1 inhibition blocks growth of RB1-positive triple negative breast cancer. Nat Commun 2020;11:4205.
33. Inoue T, Kohro T, Tanaka T, Kanki Y, Li G, Poh HM, et al. Cross-enhancement of ANGPTL4 transcription by HIF1 alpha and PPAR beta/delta is the result of the conformational proximity of two response elements. Genome Biol 2014;15:R63.
34. Legrand N, Bretscher CL, Zielke S, Wilke B, Daude M, Fritz B, et al. PPARbeta/delta recruits NCOR and regulates transcription reinitiation of ANGPTL4. Nucleic Acids Res 2019;47:9573–91.
35. Fan X, Alekseyenko AV, Wu J, Peters BA, Jacobs EJ, Gapstur SM, et al. Human oral microbiome and prospective risk for pancreatic cancer: a population-based nested case-control study. Gut 2018;67:120–7.
36. Wang X, Jia Y, Wen L, Mu W, Wu X, Liu T, et al. Porphyromonas gingivalis promotes colorectal carcinoma by activating the hematopoietic NLRP3 inflammasome. Cancer Res 2021;81:2745–59.
37. Weinert BT, Narita T, Satpathy S, Srinivasan B, Hansen BK, Scholz C, et al. Time-resolved analysis reveals rapid dynamics and broad scope of the CBP/p300 acetylome. Cell 2018;174:231–44.
38. Huang Y, Mouttet B, Warnatz HJ, Risch T, Rietmann F, Frommelt F, et al. The leukemogenic TCF3-HLF complex rewires enhancers driving cellular identity and self-renewal conferring EP300 vulnerability. Cancer Cell 2019; 36:630–44.
39. Heim CE, Bosch ME, Yamada KJ, Aldrich AL, Chaudhari SS, Klinkebiel D, et al. Lactate production by Staphylococcus aureus biofilm inhibits HDAC11 to reprogramme the host immune response during persistent infection. Nat Microbiol 2020;5:1271–84.
40. Parhi L, Alon-Maimon T, Sol A, Nejman D, Shhadeh A, Fainsod-Levi T, et al. Breast cancer colonization by Fusobacterium nucleatum accelerates tumor growth and metastatic progression. Nat Commun 2020;11:3259.
41. Xu M, Yamada M, Li M, Liu H, Chen SG, Han YW. FadA from Fusobacterium nucleatum utilizes both secreted and nonsecreted forms for functional oligomerization for attachment and invasion of host cells. J Biol Chem 2007;282: 25000–9.
42. Strauss J, Kaplan GG, Beck PL, Rioux K, Panaccione R, Devinney R, et al. Invasive potential of gut mucosa-derived Fusobacterium nucleatum positively correlates with IBD status of the host. Inflamm Bowel Dis 2011;17:1971–8.
43. Vander Heiden MG, Cantley LC, Thompson CB. Understanding the Warburg effect: the metabolic requirements of cell proliferation. Science 2009;324: 1029–33.
44. Rosenberg G, Yehezkel D, Hoffman D, Mattioli CC, Fremder M, Ben-Arosh H, et al. Host succinate is an activation signal for Salmonella virulence during intracellular infection. Science 2021;371:400–5.
45. Flynn KJ, Baxter NT, Schloss PD. Metabolic and community synergy of oral bacteria in colorectal cancer. mSphere 2016;1:e00102–16.
46. Sullivan R, Graham CH. Hypoxia-driven selection of the metastatic phenotype. Cancer Metastasis Rev 2007;26:319–31.
47. Li H, Ge C, Zhao F, Yan M, Hu C, Jia D, et al. Hypoxia-inducible factor 1 alpha-activated angiopoietin-like protein 4 contributes to tumor metastasis via vascular cell adhesion molecule-1/integrin beta1 signaling in human hepatocellular carcinoma. Hepatology 2011;54:910–9.
48. Latham T, Mackay L, Sproul D, Karim M, Culley J, Harrison DJ, et al. Lactate, a product of glycolytic metabolism, inhibits histone deacetylase activity and promotes changes in gene expression. Nucleic Acids Res 2012;40:4794–803.
49. Yang W, Yu T, Huang X, Bilotta AJ, Xu L, Lu Y, et al. Intestinal microbiota-derived short-chain fatty acids regulation of immune cell IL-22 production and gut immunity. Nat Commun 2020;11:4457.
50. Donohoe DR, Holley D, Collins LB, Montgomery SA, Whitmore AC, Hillhouse A, et al. A gnotobiotic mouse model demonstrates that dietary fiber protects against colorectal tumorigenesis in a microbiota- and butyrate-dependent manner. Cancer Discov 2014;4:1387–97.